Supplementary Information

Dendritic nanoporous nickel oxides for a supercapacitor prepared by galvanic displacement reaction with chlorine ions as an accelerator

Kai Zhuo,[a1] Myung-Gi Jeong,[a1] Chan-Hwa Chung[*a,b]

[a] *School of Chemical Engineering, Sungkyunkwan University, Suwon 440-746, Republic of Korea*
[b] *Farad Materials, Co. Ltd., 300 Chunchun-dong Jangan-ku, Suwon 440-746, Republic of Korea*
[1] *These authors contributed equally on this work.*

Fax: (+82) 31-290-7272;
Tel: (+82) 31-290-7260;
E-mail: chchung@skku.edu

The morphology of porous Ni and Ni-Sn electrodes was analyzed by JEOL JSM-7000F (Japan) field effect scanning electron microscope (FESEM) and transmission electron microscopy (TEM) (JEOL JEM-2100F, Japan). The X-ray diffractometry (XRD) (Bruker AXS D8 Discover (Germany) with Cu Kα radiation at 40 kV and 40 mA) was also employed to characterize the structural properties. The electrochemical performance and galvanostatic charge/discharge was evaluated with an electrochemical workstation (Zahner® Elektric IM6ex, Germany) and a Potentiostat/Galvanostat WPG 100 (Wonatech, Korea), respectively.

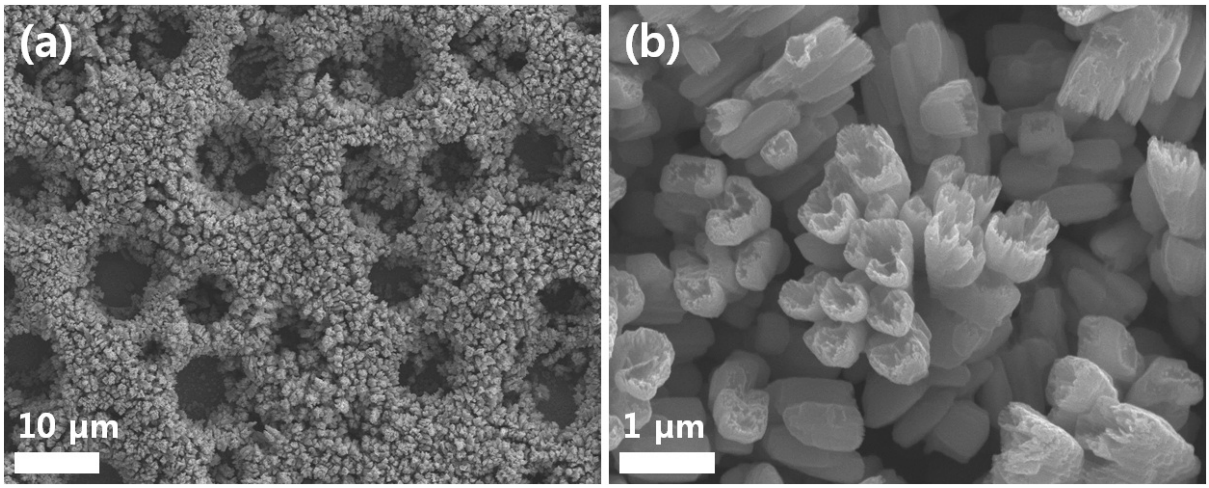

Fig. S1 FESEM images of (a) top surface of porous Ni-Sn film prepared by dynamic hydrogen template in an electrolyte containing 0.2M $NiCl_2 \cdot 6H_2O$, 0.02M $SnCl_2 \cdot 2H_2O$, and 1M H_2SO_4, (b) where the aggregated tube-like morphology is evident.

The feature of the dendritic morphology is strongly affected and needed to be optimized by content of metal ions and H^+ ions in an acidic electrolyte. The more metal ions and H^+ ions lead to the faster galvanic displacement reaction and hydrogen evolution reaction. The Fig. S2 shows the FESEM images of nanoporous Ni powders obtained by different electrolytes of (a) 1M H_2SO_4 and (b) 0.2M H_2SO_4. As shown in Fig. S2(b), in lower content of H^+ ion, the dendritic structure is well aligned and

longer in length whereas the reaction rate is much slower. When the concentration of Cl^- ions by addition of 2M NaCl was increased, the galvanic displacement reaction involving hydrogen evolution was accelerated drastically and the dendritic growth was hardly maintained in nanoporous Ni as shown in Fig. S3. This phenomenon was caused by insufficient time for continuous growth of aggregated metal atoms along the axis.

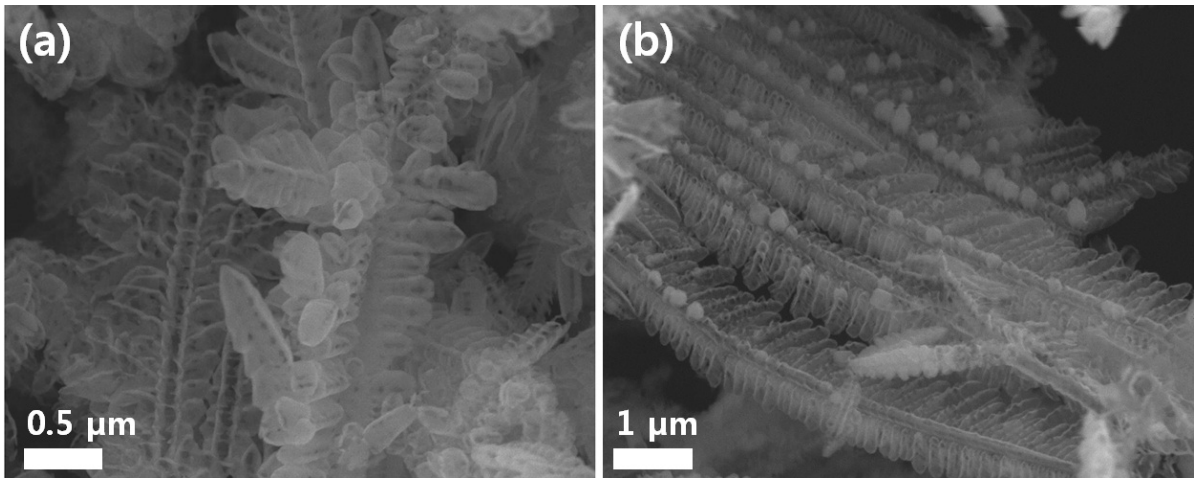

Fig. S2 FESEM images of dendritic nanoporous Ni obtained after galvanic displacement reaction involving hydrogen evolution process followed Cu-dealloying in an electrolyte with (a) 1M H_2SO_4 and (b) 0.2M H_2SO_4, respectively.

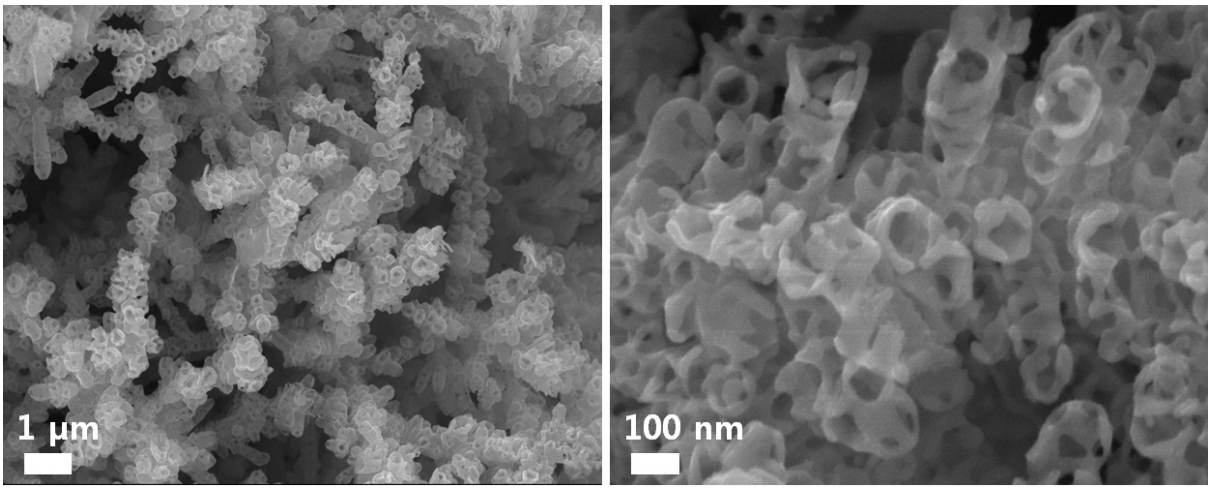

Fig. S3 FESEM images of dendritic nanoporous Ni prepared by addition of Cl^- ions with 2M NaCl.

The Fig. S5 presents XRD patterns of nanoporous Ni-(Cu) powders before and after copper dealloying from dendritic Ni-Cu alloy. The peak splitting of Ni-Cu alloy occurs in (111), (200), and (220) as well as the Cu_2O (220) peak as noted in Fig. S5(a). This indicates that Ni-Cu alloy was presented with segregated copper-rich and nickel-rich phases. In Fig. S5(b), there is no evidence of copper peak on Cu-dealloyed nanoporous Ni, which confirms that the copper was removed and only the nickel is left behind by dealloying process. After the oxidation at 200℃ in air, the NiO phases of (222), (400), (440), (622) and (444) are evident at 37.3°, 43.3°, 62.9°, 75.4° and 79.4°, respectively, as shown in Fig. S6.

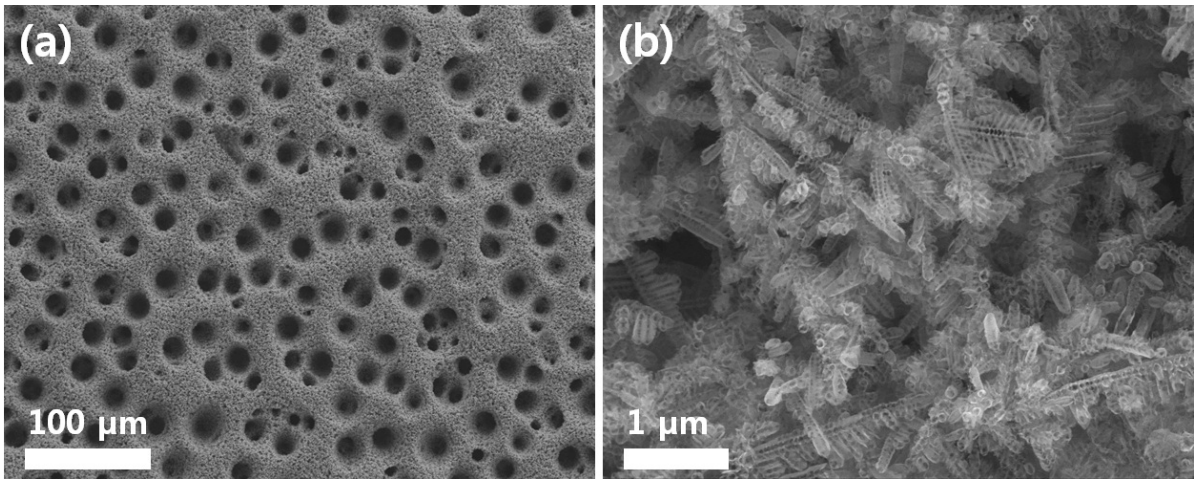

Fig. S4 FESEM images of (a) top surface of nanoporous Ni-(Cu) foam deposited by dynamic hydrogen template followed by copper dealloying, with the electrolyte of 0.2M $NiCl_2 \cdot 6H_2O$, 0.01M, $CuSO_4 \cdot 5H_2O$, and 1M H_2SO_4, (b) where the dendritic nanoporous morphology is also evident.

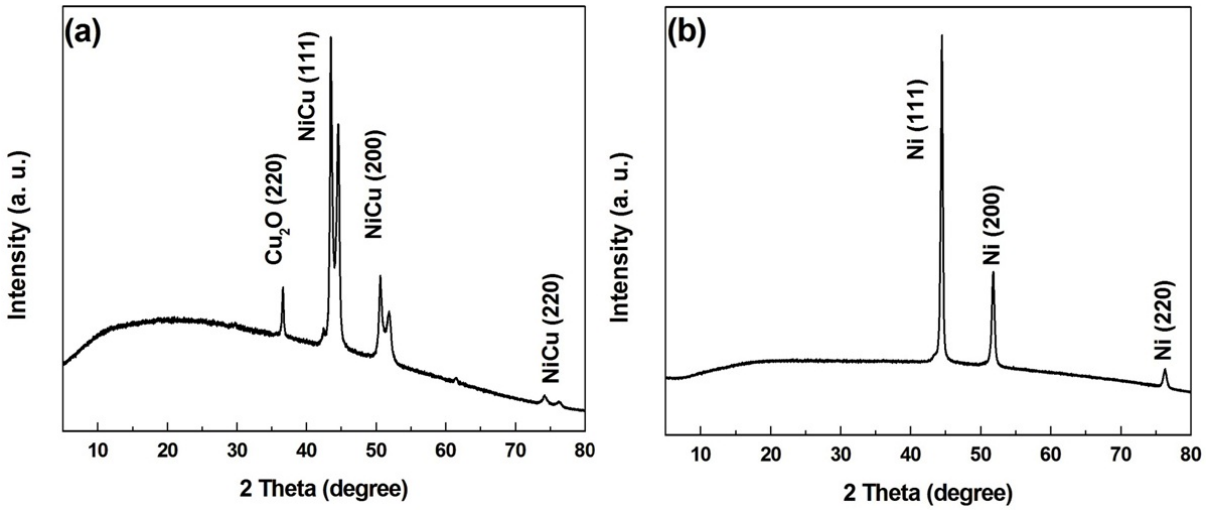

Fig. S5 XRD peaks of dendritic Ni-Cu alloy prepared by galvanic displacement reaction involving hydrogen evolution process, (a) before and (b) after dealloying of copper.

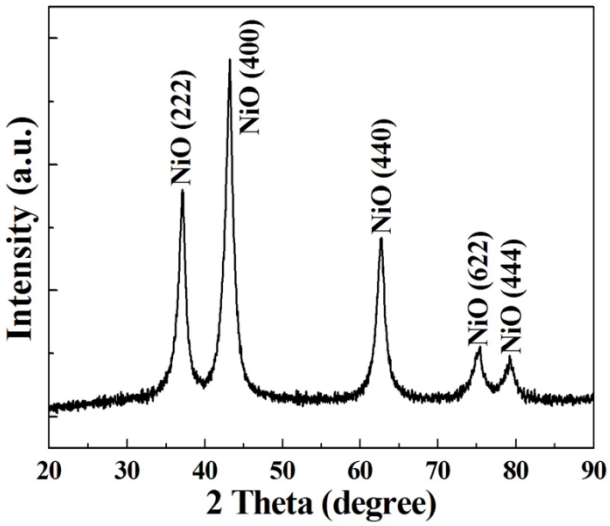

Fig. S6 XRD peaks of Ni oxide powders obtained from Ni-(Cu) after Cu de-alloying and oxidation process at 200℃ in air.

The specific capacitances calculated using CV data with various scan rates have been plotted in Fig. S7. For the Cu-dealloyed nanoporous Ni, the specific capacitance obtained from CV data was 422.8 F g^{-1}, whereas it was 442 F g^{-1} from charge-discharge experiments. The tube-like Ni-Sn also shows small difference between those values of 404.4 F g^{-1} and 397 F g^{-1}, respectively.

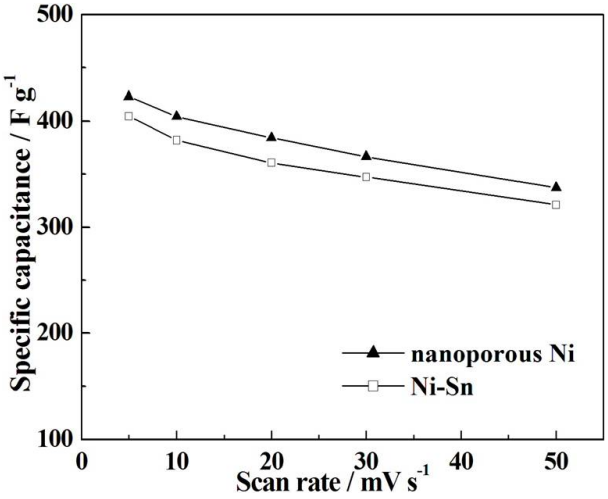

Fig. S7 The specific capacitance of Ni-Sn and Cu-dealloyed nanoporous Ni powders calculated by cyclic voltammetry analysis.

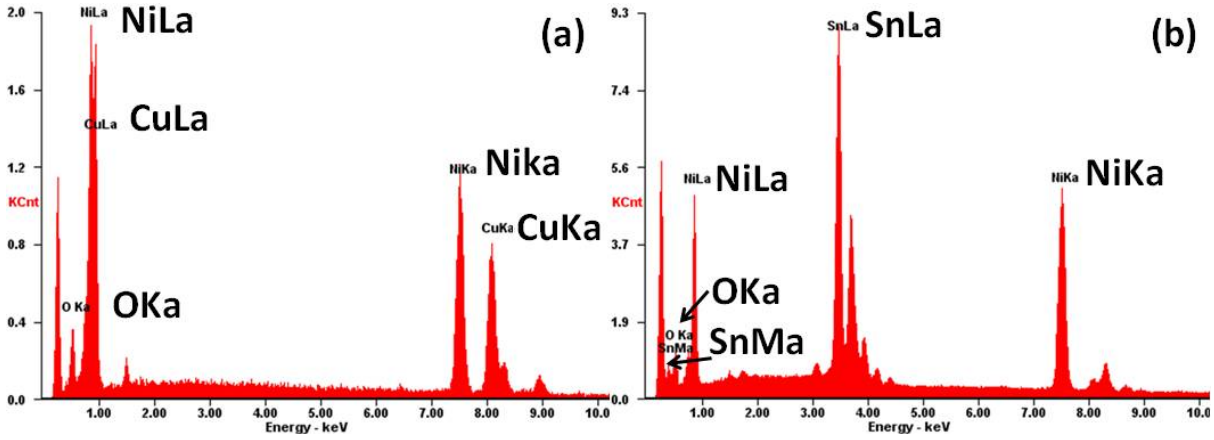

Fig. S8 Energy dispersive X-ray analysis (EDX) data of dendritic (a) Ni-Cu and (b) Ni-Sn powders.

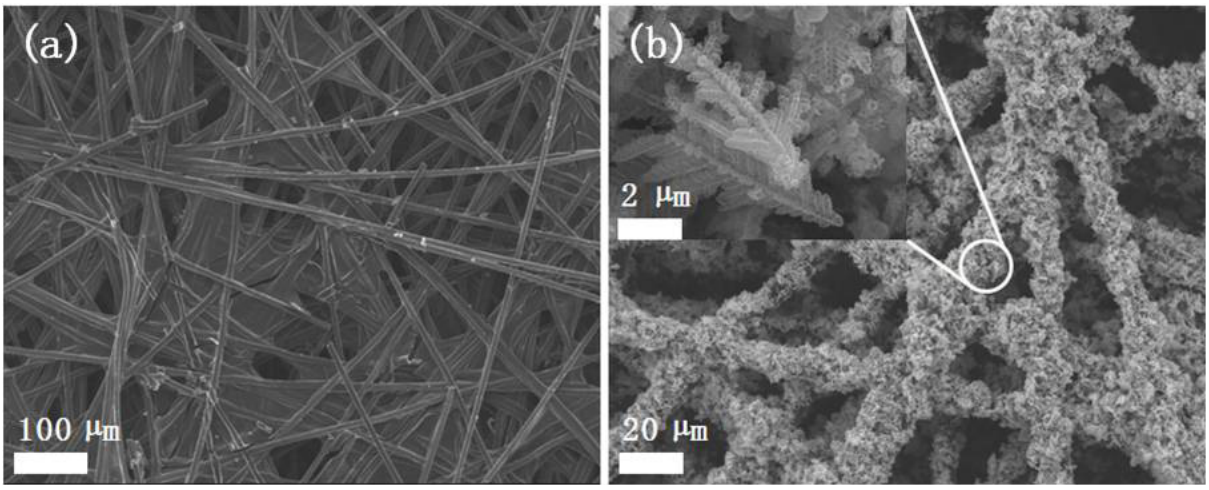

Fig. S9 FESEM image of (a) a carbon paper as current collector and (b) nanoporous Ni powder sprayed on carbon paper to measure its electrochemical performance.

As a control experiment, we have performed additional experiment of charge-discharge cycles on blank carbon paper. The 1cm×1.5cm of carbon paper is employed in 1M KOH electrolyte, and the 150 μA of current has been applied (corresponding to 7.5 mA/g of current density). The average charge-discharge cycle takes only about 0.36 seconds, as shown in Fig. S10. With the average value during 10 cycles, the specific capacitance is calculated to be 4.09 F g^{-1}. Base on the comparison of it with dendritic powders' value (~above 400 F g^{-1}), the effect of carbon paper can be negligible.

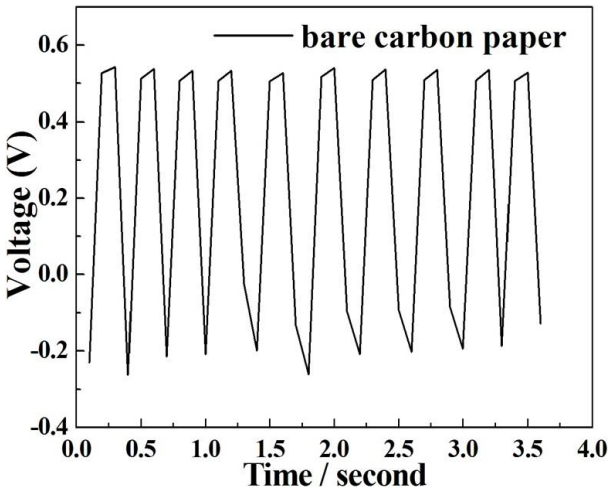

Fig. S10 The charge-discharge performance of bare-carbon paper in 1M KOH electrolyte at 7.5mA·g^{-1}.